Hindawi
International Journal of Antennas and Propagation
Volume 2022, Article ID 5412200, 12 pages
https://doi.org/10.1155/2022/5412200

Research Article

A New Approach for Calculation of Metamaterial Printed Fractal Antenna Using Galerkin's Method

Amjad S. Saedy, Al-Samawal. Saleh, and Sadiq. Ali

Department of Communication Engineering, Faculty of Mechanical and Electrical Engineering, Tishreen University, Lattakia, Syria

Correspondence should be addressed to Amjad S. Saedy; amjad.saedy@tishreen.edu.sy

Received 6 May 2022; Revised 16 September 2022; Accepted 21 September 2022; Published 13 October 2022

Academic Editor: Trushit Upadhyaya

This work provides a new approach for computing the impedance of a proposed multiband printed fractal antenna for wireless applications. Galerkin's method is applied to deduce the impedance relationship of the proposed structure and then compute the return loss verses frequency by converting the impedance matrix of the proposed antenna [Z] to the scattering matrix [S]. This model is developed in order to study the impedance of the proposed antenna after adding a metamaterial structure in the antenna substrate. The obtained model is able to determine the resonant frequencies and the return loss of the proposed antenna. The model is also able to define the changes in these values when the dimensions of the proposed structure change. The proposed antenna provides multiband wireless applications in the (1–10) GHz frequency band, and the return loss of the proposed fractal antenna has been improved using negative permittivity and negative permeability metamaterial structure.

1. Introduction

The technical development in wireless communications creates multiapplications devices.

These devices work on various frequencies or multiband frequencies for applications like Bluetooth, WiFi, WLAN, and WiMAX [1]. These applications require a new type of printed antenna that works on wide band frequencies or multiband frequencies. Fractal, multiscale antenna and multidimension antennas are the common proposed types [1].

Fractal geometry has been used to design multiband antennas that resonate at different frequencies according to the effective lengths of the fractal structure.

These antennas are characterized by different effective dimensions or several slots with a specific arrangement, printed on a substrate consisting of a material with a specified dielectric constant [2, 3].

Various fractal structures, such as Cantor Bar, Koch, Tree, Minkowski, and Hilbert, were used for designing multiband antennas [4–6].

Dual-band and triple-band fractal patch antennas were proposed in [7]. The structure was based on the Sierpinski carpet fractal, while a defected ground structure and a reflector plane were utilized for enhancing the gain of the antenna [7].

Abdaljabar et al. [8] proposed a microstrip fractal patch antenna with a COVID-19 shape in order to create a miniature antenna for dual-band wireless, satellite, and radar applications.

The proposed antenna operated and resonated on two frequencies of 7.5 GHz and 17 GHz within C and Ku bands, respectively.

Souza et al. [9] presented a dual-band small-size microstrip antenna. Koch fractal contour structure was used to reduce the antenna size by 70%.

Some studies suggested fractal patch antenna shapes which have different slots like triangular, rectangular, square and hexagonal. For example, a rectangular Minkowski fractal slot antenna was proposed in [10]. The proposed fractal antenna was used to increase the effective area and bandwidth of the antenna. This antenna had a compact size

where the number of operating frequencies and the gain were higher than the reference antennas.

Wide slot triband antenna for wireless applications was proposed in [11]. The proposed structure consisted of a wide circular and rectangular slot. Those slots were placed in the design to excite multiple resonating modes, at different frequencies.

Recently, great interest has emerged in the interaction of electromagnetic waves with manufactured structures that provide negative electrical permittivity and negative magnetic permeability at certain frequencies. These structures are called metamaterials [12].

Metamaterial structure has the property that controls the direction of electromagnetic radiation to gather the energy in a small angular domain [12, 13]. Besides that, the metamaterials antennas have been used to improve the performance of the antenna because it has unique band gap features and periodic structures. The metamaterials antenna has a structure that saves and re-radiates energy making its size small and behaves as a larger antenna [13]. For those previous reasons, the metamaterial structures have been used to increase the radiation power of the printed antenna.

A metamaterial, inspired tapered patch antenna operating in 2.5 GHz, 3.5 GHz, 4.6 GHz, and 5.8 GHz, was proposed in [14]. Circular split-ring resonator (CSRR) metamaterial structure was placed near the radiating edges of the antenna to enhance the return loss of the antenna.

Researchers in [15] introduced an antenna which has a rectangular patch on the front side along with two CSRRs and a metamaterial cover on the back side. Their approach was intended to improve the performance of the antenna for 2.4 GHz WiFi applications.

In [16], metamaterial fractal defected ground structure was presented to obtain multiband wireless applications (2.8 GHz, 4.1–4.45 GHz, and 5.6 GHz). Koch snowflake fractal was etched from the four edges of the resonating patch to improve return loss. A double negative metamaterial unit cell was used to increase the gain and radiation efficiency of a compact patch antenna at the resonance frequencies.

Researchers in [17] proposed a design of an ultra-wideband fractal antenna. Metamaterial was located in the ground plane in order to enhance the gain and directivity of the antenna.

Paper [18] presents a dual-band planar antenna for GSM and WiMAX applications. The researcher suggested adding two SRR cells to improve the directivity and gain and a partial ground plane to improve bandwidth.

In paper [19], the ground plane was engineered by the placement of an SRR array to induce additional resonance due to the occurrence of magnetic dipole moment.

Square-shaped SRR was proposed in [20] to obtain a dual-band fractal printed antenna operation with wideband operation at the higher frequency band.

Most of the previous studies used simulators only to design the proposed antennas, and these antennas operated at specific frequencies.

The main objective of this research is to present a mathematical model in order to design a multiband metamaterial printed fractal antenna. The proposed mathematical model gives wide design powers so that the antenna resonant frequencies can be changed according to the required application.

2. Materials and Methods

2.1. Galerkin's Method. Galerkin's method aims to study the discontinuity in the waveguide and calculate the equivalent impedance. This is done by equating the discontinuity in the waveguide in an electrical circuit and then calculating the equivalent impedance of that circuit using Kershof laws [21, 22].

The discontinuity in the waveguide occurs due to a sudden change in waveguide dimensions. However, it can be caused due to a change in the type of the material. This discontinuity affects the propagation of modes in waveguide [21].

2.2. Design of Printed Antenna Using Galerkin's Method. We assume that the patch antenna is placed in a waveguide, as shown in Figure 1(a), and thus a discontinuity will occur in this waveguide. The impedance of the equivalent circuit (Figure 1(b)) is calculated using the Galerkin method. After that, the antenna impedance versus frequency ($Z = R + j\,\mathrm{X}$) is studied. The resonant frequency of the antenna is the frequency at which the true part of the impedance is the greatest and the imaginary part is the least [21].

The return loss S_{11} versus frequency is studied by converting the impedance matrix $[Z]$ of the antenna to the scattering matrix $[S]$, to determine resonant frequencies at which the antenna can radiate or receive energy [23, 24].

Figure 1 shows the discontinuity in the waveguide and the equivalent electrical circuit.

2.3. The Impedance Relation. From the equivalent electrical circuit, equations (1) and (2) can be derived as follows:

$$E = E_1 = E_2, \tag{1}$$

$$J = -J_1 - J_2 + \left(Y_1 + Y_2\right) * E. \tag{2}$$

Equations (1) and (2) can be written as follows:

$$\begin{vmatrix} E_1 \\ E_2 \\ J \end{vmatrix} = \begin{vmatrix} 0 & 0 & 1 \\ 0 & 0 & 1 \\ -1 & -1 & Y_1 + Y_2 \end{vmatrix} \begin{vmatrix} J_1 \\ J_2 \\ E \end{vmatrix}, \tag{3}$$

$$\begin{aligned} E_1 &= V_1 f_1' \Rightarrow J_1 \\ &= I_1 f_1' E_2 \\ &= V_2 f_1 \Rightarrow J_2 \\ &= I_2 f_1, \\ E &= \sum_q X_q f_q. \end{aligned} \tag{4}$$

V_1 and V_2 are the voltages resulting from the propagating modes in the first and second waveguide. X_q is the

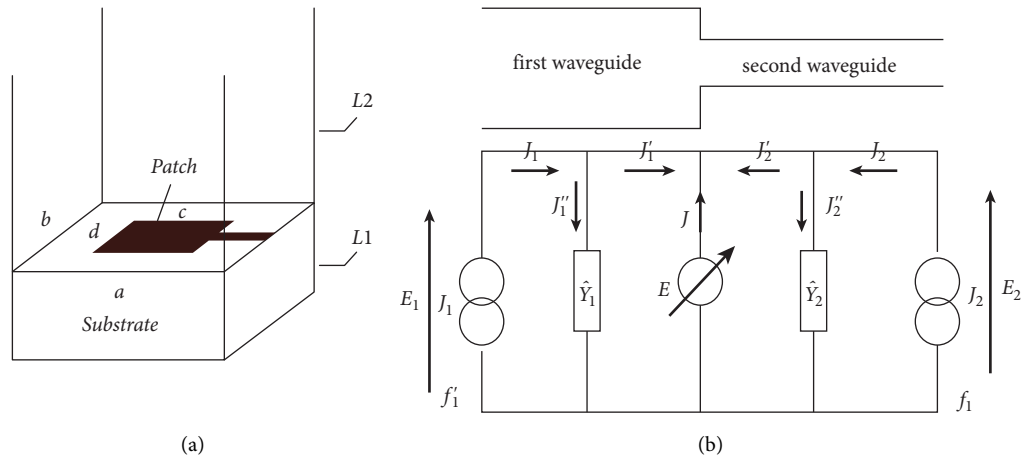

Figure 1: Discontinuity in the waveguide (a) and equivalent circuit (b). a, b: the dimensions of the first waveguide (the substrate of the antenna). c, d: the dimensions of the second waveguide (patch antenna). Y_1, Y_2: the equivalent permittivity expressing the first and second waveguide. J_1: the current resulting from the propagating modes in the first waveguide. J_2: the current resulting from the propagating modes in the second waveguide. E_1: the voltage source resulting from the propagating modes in the first waveguide. E_2: The voltage source resulting from the propagating modes in the second waveguide. E: the voltage source expressing the discontinuity in the waveguide.

discontinuity impedance. f_q is the propagating modes in the discontinuity region.

Therefore, equation (3) becomes as follows:

$$\begin{vmatrix} V_1 \\ V_2 \\ 0 \end{vmatrix} = \begin{vmatrix} 0 & 0 & \langle f_1'/f_p \rangle \\ 0 & 0 & \langle f_1/f_p \rangle \\ -\langle f_p/f_1' \rangle & -\langle f_p/f_1 \rangle & \langle f_p(Y_1+Y_2)f_q \rangle \end{vmatrix} \begin{vmatrix} I_1 \\ I_2 \\ \sum_q X_q \end{vmatrix}. \tag{5}$$

$\langle f_1'/f_p \rangle$ is the propagating modes in the first waveguide. $\langle f_1/f_p \rangle$ is the propagating modes in the second waveguide. $\langle f_p(Y_1+Y_2)f_q \rangle$ is the permittivity of the circuit and all propagating modes in this circuit. The matrix equation (5) can be rewritten into the following matrix equation:

$$\begin{vmatrix} V_1 \\ V_2 \\ 0 \end{vmatrix} = \begin{vmatrix} 0 & 0 & [A] \\ 0 & 0 & [B] \\ -[A]^t & -[B]^t & [D] \end{vmatrix} \begin{vmatrix} I_1 \\ I_2 \\ [X] \end{vmatrix}$$

$$[A]^t I_1 + [B]^t I_2 = [D][X] \Rightarrow [X] = \left[[D]^{-1} [A]^t [B]^t \right] \begin{bmatrix} I_1 \\ I_2 \end{bmatrix} \Rightarrow$$

$$\begin{bmatrix} V_1 \\ V_2 \end{bmatrix} = \begin{bmatrix} [A] \\ [B] \end{bmatrix} [X] \Rightarrow \begin{bmatrix} V_1 \\ V_2 \end{bmatrix} = \begin{bmatrix} [A] \\ [B] \end{bmatrix} [D]^{-1} \left[[A]^t [B]^t \right] \begin{bmatrix} I_1 \\ I_2 \end{bmatrix}$$

$$\Rightarrow [Z] = \begin{bmatrix} [A] \\ [B] \end{bmatrix} [D]^{-1} \left[[A]^t [B]^t \right]. \tag{6}$$

(1) $[A]$ is a matrix related to the frequencies propagated in the first waveguide.

(2) $[B]$ is a matrix related to the frequencies propagated in the second waveguide.

(3) $[D]$ is a matrix related to the frequencies propagated in the first and second waveguide and the permittivity of the first and second waveguide, it is given by equations (7)–(10).

$$D = \sum \frac{\left| \langle f_p/f_{TE} \rangle \right|^2}{y_1^{TE} + y_2^{TE}} + \sum \frac{\left| \langle f_p/f_{Tm} \rangle \right|^2}{y_1^{TM} + y_2^{TM}}, \tag{7}$$

$$y_1^{TE} = \left(\frac{\gamma_1}{j\omega\mu_0} \right) \cot(\gamma_1 l_1),$$
$$y_2^{TE} = \left(\frac{\gamma_2}{j\omega\mu_0} \right) \cot(\gamma_2 l_2), \tag{8}$$

$$y_1^{TM} = \left(\frac{j\omega\varepsilon_0\varepsilon_r}{\gamma_1} \right) \cot(\gamma_1 l_1),$$
$$y_2^{TM} = \left(\frac{j\omega\varepsilon_0}{\gamma_2} \right) \cot(\gamma_2 l_2), \tag{9}$$

$$\gamma_2^2 = \frac{m^2\pi^2}{a^2} + \frac{n^2\pi^2}{b^2} - k_o^2, \gamma_1^2 = \frac{m^2\pi^2}{a^2} + \frac{n^2\pi^2}{b^2} - k_0^2\varepsilon_r, \tag{10}$$

$$w = 2\pi f,$$
$$k_0 = \frac{2\pi}{\lambda},$$
$$\mu_0 = 4\pi 10^{-7},$$
$$\varepsilon_0 = \frac{1}{36\pi 10^9}. \tag{11}$$

$\lambda[m]$ is the wavelength. $c[m/\text{sec}]$ is the speed of light in a vacuum. $f[HZ]$ is the frequency of the antenna. $l_1[m]$ is the

Table 1: Dimensions of the proposed fractal antenna in mm.

L	W	ε_r	Sub h	Sub y	Sub x	L_1	W_1
49.4	41.4	2.2	1.57	123.4	83.6	38.075	4.85

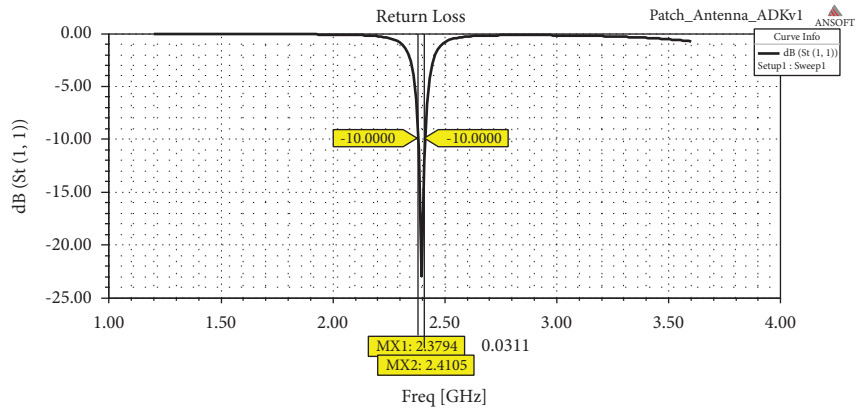

Figure 2: The return loss versus frequency of the reference antenna ($f = 2.4$ GHz and $S_{11} = -22$ dB).

thickness of the substrate, $l_2 \gg l_1$. ε_r is the relative dielectric constant of the substrate. γ_1 an dγ_2 are the propagation constants.

2.4. Antenna Geometry and Design. The proposed fractal antenna is designed according to the following stages.

2.4.1. First Stage: Design of a Reference Antenna Operating at a Frequency of 2.4 GHz. According to [24], the dimensions of reference patch antenna using transmission line theory are calculated and shown in Table 1.

The antenna is designed on substrate ($\varepsilon_r = 2.2$) with dimensions $123.4 \times 83.6 \times 1.57\ \text{mm}^3$.

Table 1 shows the dimensions of the reference antenna in mm.

The reference antenna is simulated using HFSS software, and the return loss versus frequency is depicted in Figure 2.

2.4.2. Second Stage: Design of Multiband Fractal Antenna. The proposed fractal antenna is characterized by different effective dimensions or several slots with a specific arrangement as shown in Figure 3(b).

Fractal antenna structure is proposed using the Cantor Bar towards the two axes (X, Y). The antenna patch is divided into four smaller self-similar segments as shown in Figure 3(a), with a scaling ratio of 1/3. Then, a metal strip in the form of a sign (+) is added within the four segments connecting the antenna feeding line to this strip [25].

The dimensions of this metal strip are $X_1 = \text{L}/3.5 = 10.97$ mm and $Y_1 = W/3.5 = 9.2$ mm.

3. Results and Discussion

3.1. Design of Proposed Fractal Antenna Using Galerkin Method. Galerkin's method is applied to the proposed fractal antenna. The value of the equivalent impedance of the antenna versus frequency is then calculated.

The resonant frequency of the antenna is the frequency at which the true part of the impedance is the greatest and the imaginary part is the least.

Figures 4(a)–4(c) show the resonant frequencies of the proposed fractal antenna 2.68 GHz, 5.15 GHz, and 7.72 GHz.

3.2. Return Loss. After computing the impedance matrix [Z] of the proposed antenna, equation (12) is used to compute the return loss S_{11} versus frequency [23, 24].

$$s_{11} = \frac{(z_{11})(z_{22} + z_{02}) - z_{12}z_{21}}{(z_{11} - z_{01})(z_{22} + z_{02}) - z_{12}z_{21}}. \tag{12}$$

Figures 5(a)–5(c) show the value of the return loss of the proposed fractal antenna.

The return loss of the proposed fractal antenna is −13 dB, −18 dB, and −24 dB at 2.68 GHz, 5.15 GHz, and 7.72 GHz, respectively. As a result, the proposed fractal antenna resonates at three frequency bands, thus increasing the number of resonant frequencies in which the antenna can radiate or receive energy (i.e., improving the bandwidth of the antenna).

3.3. Metamaterial Structure Design. The metamaterial structure consists of Split-Ring Resonators (SRRs) with straight metallic wires. The SRR cell consists of two rings made of a non-magnetic metal that is folded concentrically with a slit in each of them, as shown in Figure 6 [12].

Table 2 shows the dimensions of the proposed metamaterial structure which is used in this work. This structure gives negative electrical permittivity and negative magnetic permeability in the (4.8–5.8) GHz frequency band. The thickness of the substrate (h_2) is 0.7 mm.

The S-parameters (reflection coefficient S_{11} and transmission coefficient S_{21}) of the metamaterial structure are

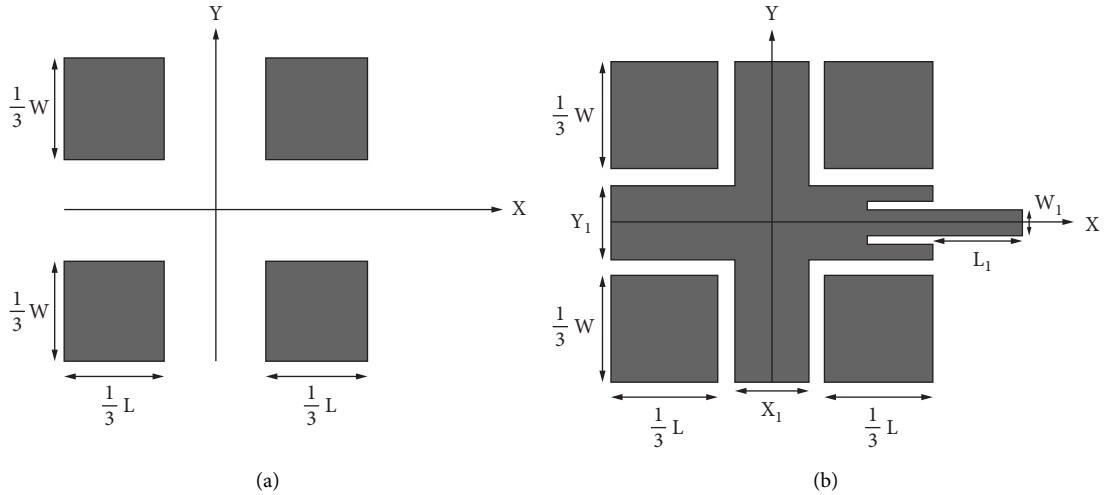

FIGURE 3: The proposed fractal antenna.

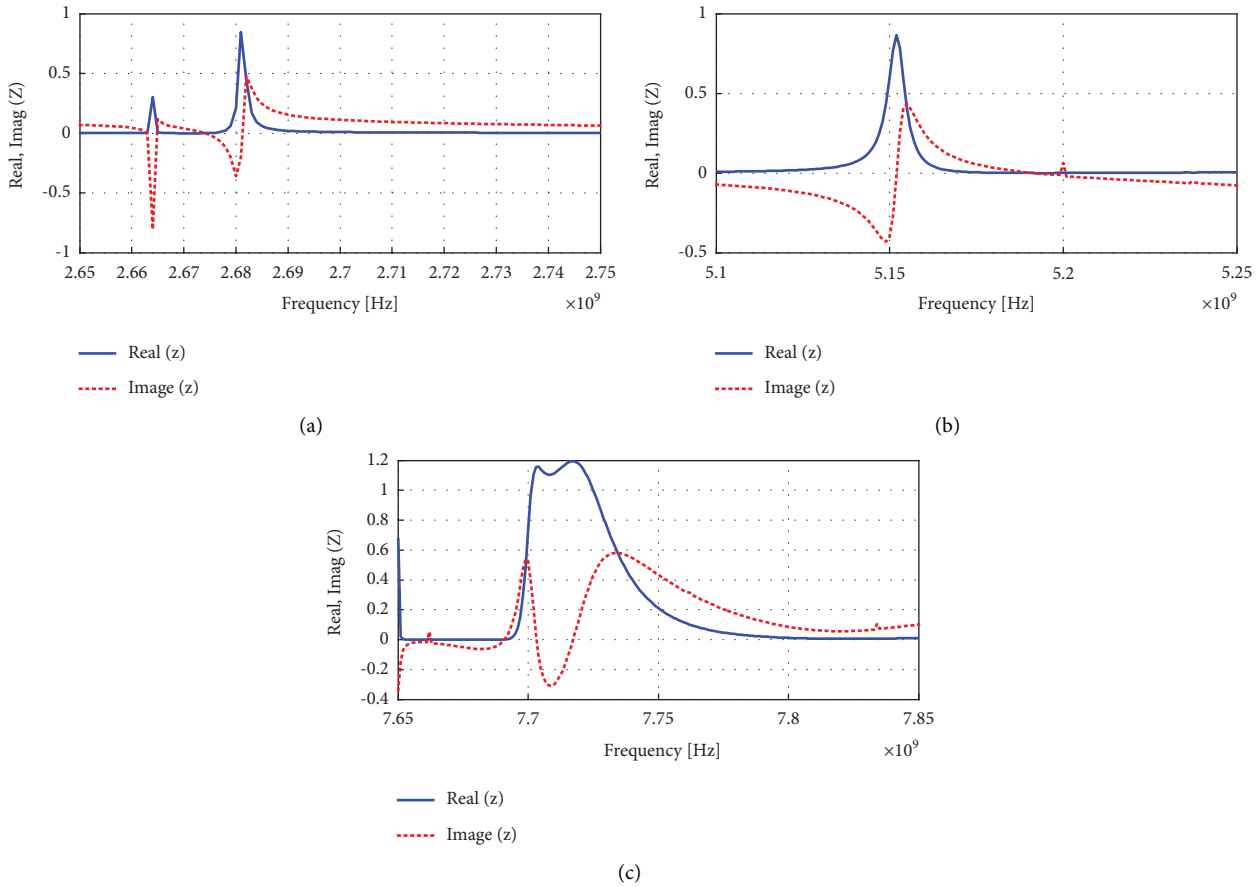

FIGURE 4: (a) The first resonant frequency of the proposed fractal antenna ($f = 2.68$ GHz) . (b) The second resonant frequency of the proposed fractal antenna ($f = 5.15$ GHz). (c) The third resonant frequency of the proposed fractal antenna ($f = 7.72$ GHz).

analyzed using HFSS software; then, the effective parameters of the metamaterial structure (such as the electrical permittivity (ε), magnetic permeability (μ), impedance (z), and the refractive index (n)) are calculated using Matlab program [16], as shown in Figure 7. As it can be seen, the real parts of the electrical permittivity, magnetic permeability, and refractive index reach a negative value in the (4.8–5.8) GHz band.

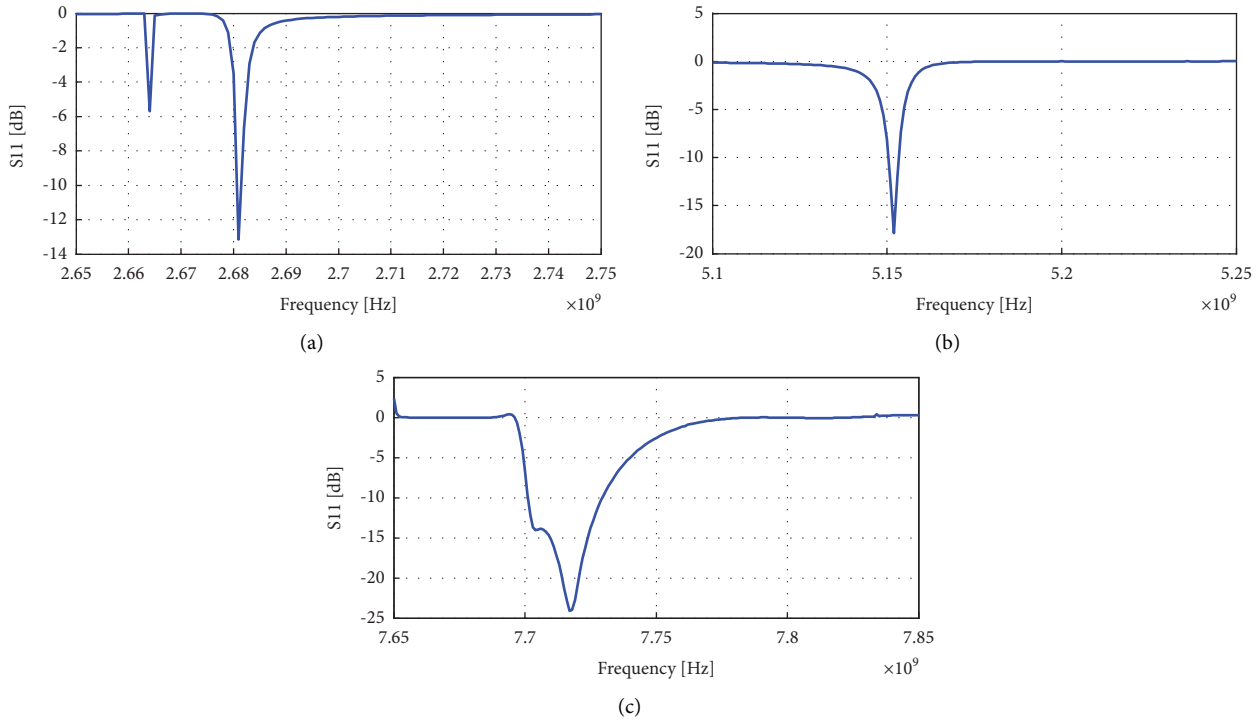

Figure 5: (a) Return loss of the proposed antenna ($f = 2.68$ GHz and $S_{11} = -13$ dB). (b) Return loss of the proposed antenna ($f = 5.15$ GHz and $S_{11} = -18$ dB). (c) Return loss of the proposed antenna ($f = 7.72$ GHz and $S_{11} = -24$ dB).

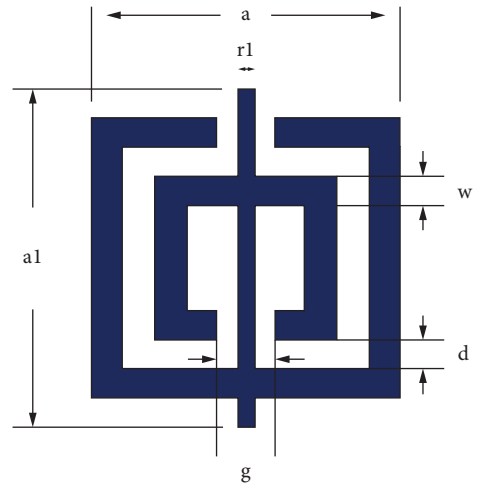

Figure 6: Metamaterial structure.

Table 2: The dimensions of the proposed metamaterial structure in mm.

a	g	w	d	a_1	r_1	h_2	ε_r
5	0.6	0.5	0.5	5.2	0.4	0.7	2.2

3.4. Metamaterial Fractal Antenna Design. Figure 8 shows the proposed metamaterial fractal antenna.

The proposed metamaterial structure is placed in the substrate of the proposed antenna under the patch, at a height of $h_2 = 0.7$ mm above the ground plane, as shown in Figure 9.

3.5. Effective Permittivity and Effective Permeability of the Metamaterial Substrate. The addition of metamaterial structure in the substrate of the proposed fractal antenna will produce a negative electrical permittivity ($\varepsilon_2 < 0$) and negative magnetic permeability ($\mu_2 < 0$) in the (4.8–5.8) GHz frequency band, as shown in Figure 7.

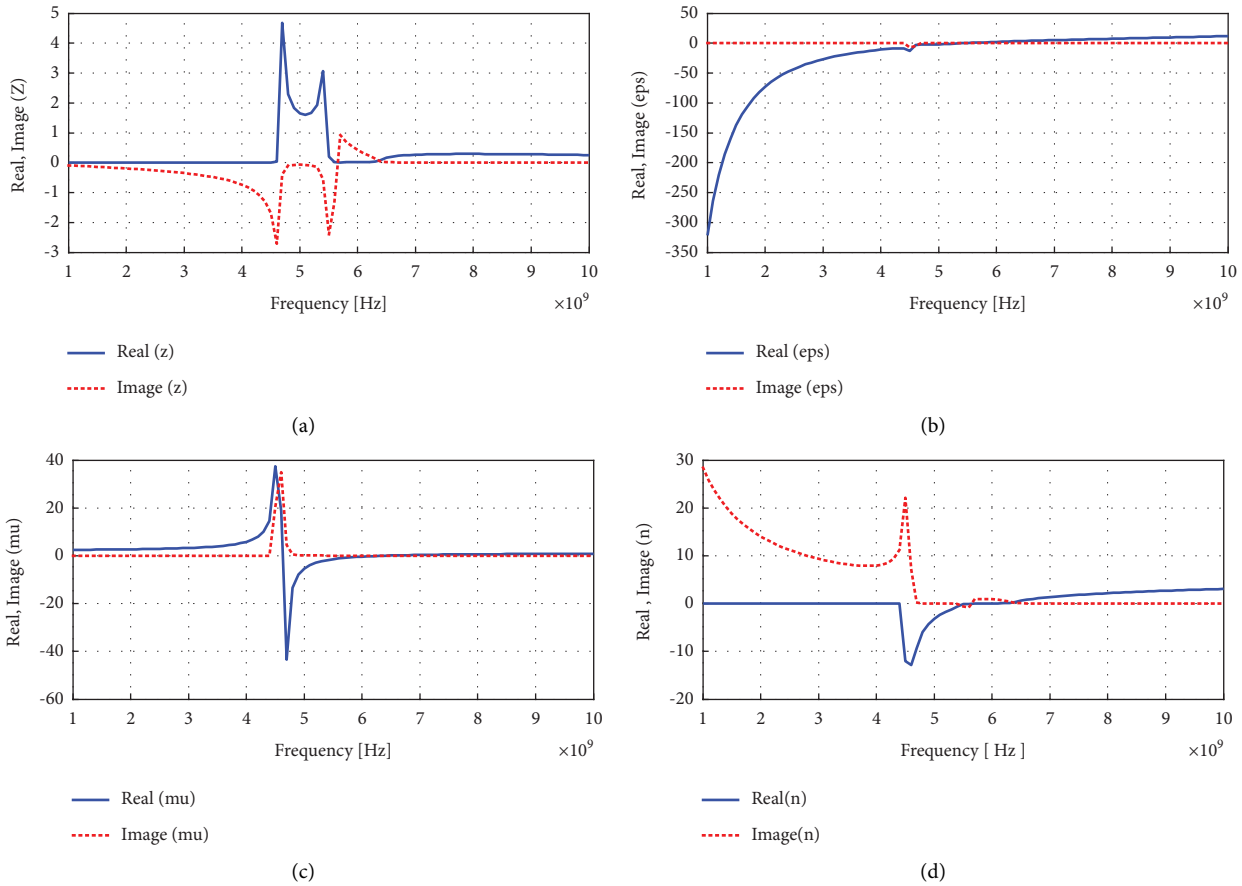

Figure 7: (a) The impedance, (b) electrical permittivity, (c) magnetic permeability, and (d) refractive index, of the proposed metamaterial structure.

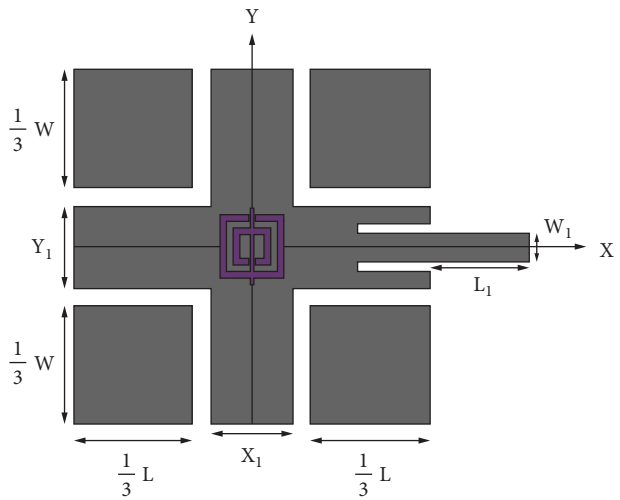

Figure 8: The proposed metamaterial fractal antenna.

Figure 9: The substrate of the proposed metamaterial fractal antenna. (a) Front view. (b) Top view.

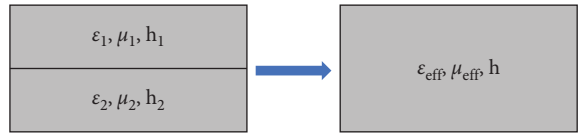

Figure 10: The double substrate and its equivalent single layer model.

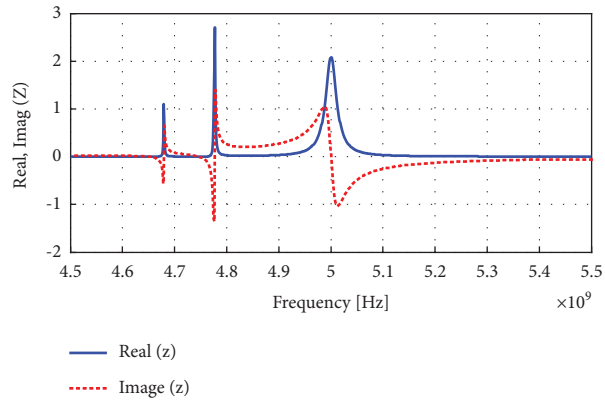

Figure 11: Frequencies of the metamaterial fractal antenna.

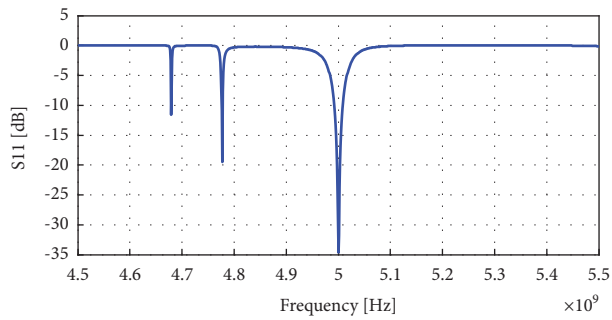

Figure 12: Return loss of the fractal antenna with loaded metamaterial structure.

Therefore, the effective electrical permittivity (ε_{eff}) and effective magnetic permeability (μ_{eff}) of the equivalent substrate must be calculated using following equations [26, 27], as shown in Figure (10):

$$\frac{1}{\varepsilon_{\text{eff}}} = \sum_{n=1}^{N} \frac{1}{\varepsilon_n} \frac{h_n}{h_t}, \qquad \frac{1}{\mu_{\text{eff}}} = \sum_{n=1}^{N} \frac{1}{\mu_n} \frac{h_n}{h_t}. \tag{13}$$

After the development of Galerkin's method for computing the impedance and return loss, we obtain the frequencies as shown in Figure 11.

The return loss versus frequency of the proposed metamaterial fractal antenna is depicted in Figure 12; the figure shows that the return loss is −35 dB at 5 GHz.

Figure 13 shows a comparison of the return loss of the proposed antenna with and without metamaterial structure.

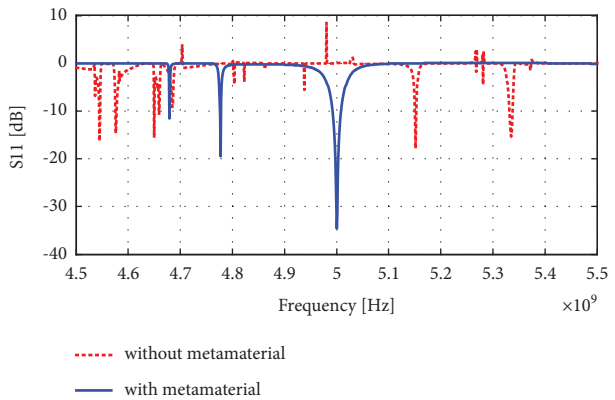

Figure 13: Comparison of return loss of the proposed antenna with and without metamaterial.

The return loss has been improved by about 17 dB, using the proposed metamaterial structure.

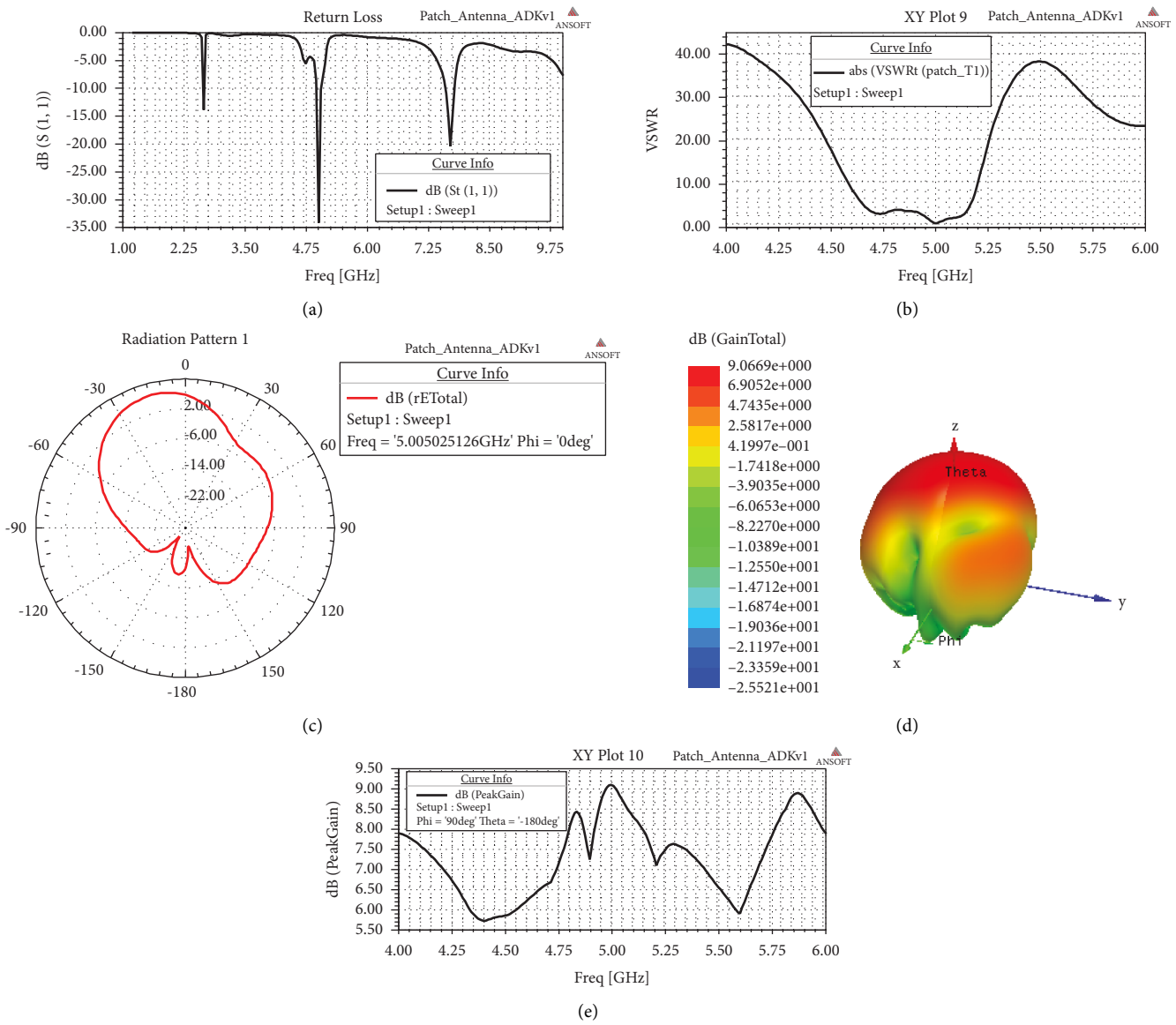

Figure 14: (a) Return loss of the metamaterial fractal antenna using HFSS simulator. (b) VSWR of the proposed antenna. (c) 2D radiation pattern of the proposed antenna at 5 GHz. (d) 3D radiation pattern and gain of the proposed antenna at 5 GHz. (e) The peak gain of the proposed antenna.

To prove the obtained results of the designed model, HFSS simulator is used to design the proposed antenna.

Figure 14(a) illustrates the return loss of the proposed antenna using HFSS simulator.

We notice that the obtained parameters of the proposed antenna are good compared to those of the other previous studies.

According to simulations, there are resonant frequencies at 2.7 GHz, 5 GHz, and 7.75 GHz.

Good agreement between simulation and mathematical model results is observed.

Figure 14(b) shows the VSWR of the proposed antenna in (4–6) GHz frequency band. The simulated VSWR is 1.1 at 5 GHz.

Figure 14(e) shows the peak gain of the proposed antenna in (4–6) GHz frequency band.

The gain of the proposed antenna is 9 dB at 5 GHz.

4. Comparing the Results of This Research with a Number of Recent reference Studies

Table 3 shows a comparison of the results of this research with some reference studies that used fractal geometry and metamaterial structures in the design of printed antennas.

We notice that the obtained parameters of the proposed antenna are good compared to those of the other previous studies.

4.1. Fabrication and Measured Results. The proposed metamaterial fractal antenna has been fabricated and tested in order to validate experimentally the design approach. The fractal antenna is fabricated on substrate ($\varepsilon_{r=4.4}$) with dimensions $123.4 \times 83.6 \times 1.57\ mm^3$ as shown in Figure 15(a).

Table 3: Comparing the results of this research with a number of recent reference studies.

Ref.	Year	Resonant frequency (GHz)	Gain (dB)	Return loss (dB)	Antenna structure	Design method
8	2022	7.5 17	2.2	−35	Fractal patch antenna with a COVID-19 shape	HFSS
28	2022	3.5	2.6	−40	CSRR in the patch and 3 ∗ 3 metamaterial structures in the ground	HFSS
29	2021	7.28	10	−19	Fractal patch antenna and four SRR structures around the patch	FEKO
30	2021	2.4 5.3	2.67	−35	Sierpinski fractal antenna and ground plane with slots	CST
1	2021	2.5, 5.1 6.7, 7.7 8.6, 9.5 11.3	5.6	−13.8, −10.84 −13.48, −23.24 −12.88, −14.17 −26.09	Fractal antenna and metamaterial structure under the patch	HFSS
6	2021	2.4	6	−26	Minkowski fractal antenna and metamaterial structure under the patch	HFSS
This work	2022	2.7, 5,7.75	9	−14, −35, −20	Fractal patch antenna and metamaterial structure under the patch	HFSS and mathematical model

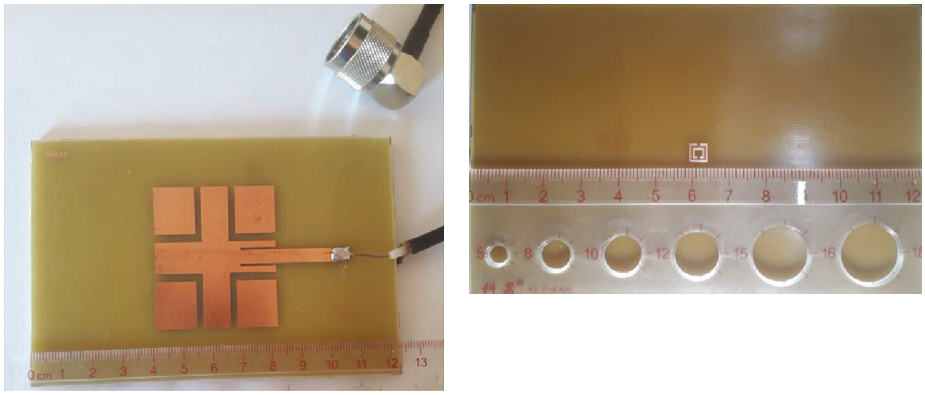

(a) (b)

Figure 15: Fabricated proposed antenna. (a) Fractal antenna. (b) Metamaterial structure.

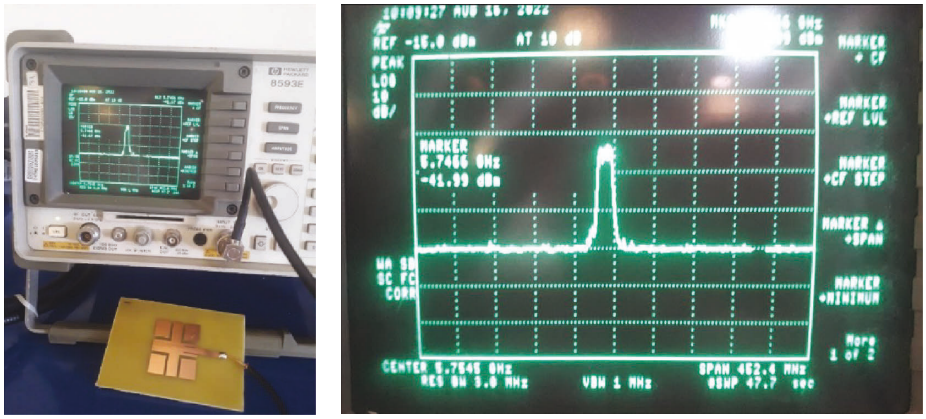

(a) (b)

Figure 16: Measurement setup for the proposed antenna.

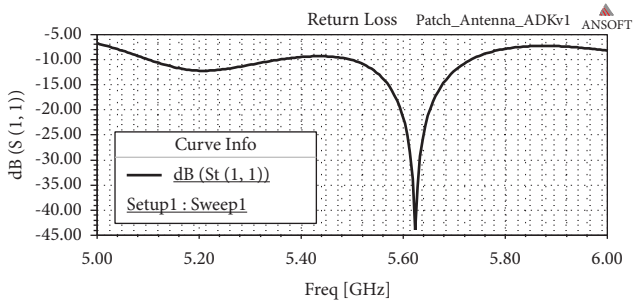

Figure 17: The return loss versus frequency of the proposed antenna using HFSS simulator (f = 5.6GHz; $S11 = -44\,dB$).

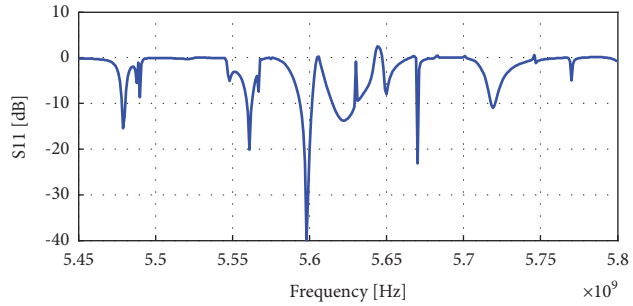

Figure 18: The return loss versus frequency of the proposed antenna using mathematical model (f = 5.6GHz; $S11 = -40\,dB$).

Table 4: Comparison between simulation, mathematical model, and measured results.

Resonant frequency (GHz)	Return loss (dB)	Design method
5.6	−44	HFSS software
5.6	−40	Mathematical model
5.74	−41.99	Measured results

The metamaterial structure is fabricated on another substrate with the same ε_r and dimensions as shown in Figure 15(b).

The resonant frequency and return loss of the proposed antenna are measured using spectrum analyzer 8593E as shown in Figure 16(a).

Figure 16(b) shows that the resonant frequency of the proposed fractal antenna is 5.7 GHz, and the return loss of the proposed fractal antenna is −41.99 dB

To prove the obtained measured results, HFSS simulator and mathematical model are used to design the proposed antenna. Figure 17 shows the return loss versus frequency of the proposed antenna using HFSS simulator, while Figure 18 illustrates the return loss versus frequency of the proposed antenna using the mathematical model.

5. Conclusions

A mathematical approach was proposed in this work for calculating the return loss and resonant frequencies of a multiband printed fractal antenna with metamaterial substrate. This model was generated by applying Galerkin's method to calculate the impedance of the proposed structure. The mathematical approach was developed to study the effect of metamaterial structure for improving the return loss of the antenna.

The return loss of the proposed fractal antenna has been improved using metamaterial structure. As a result, the radiation energy of the fractal antenna with metamaterial was greater than the energy of the fractal antenna without metamaterial.

In order to validate the proposed methodology, metamaterial fractal antenna was fabricated and tested. The simulation, mathematical model, and measured results were almost the same.

In future research, we propose to develop a mathematical approach to study the performance of the proposed fractal antenna using fractal distribution of metamaterial structures [7, 28, 29].

Data Availability

There are no datasets in this research.

Conflicts of Interest

The authors declare that there are no conflicts of interest regarding the publication of this paper.

Acknowledgments

The experiments on the fabricated fractal antenna were applied at the communication laboratory in Tishreen University by assistance of Dr. Mohammad Asaad.

References

[1] G. Ramalakshmi and P. M. Rao, "A novel metamaterial inspired iteration Koch fractal antenna for WiFi, WLAN, C band and X band wireless communications," *Journal of Physics*, Conference Series, vol. 2062, 2021.

[2] W. J. Krzysztofik, "Fractal geometry in electromagnetics applications from antenna to metamaterials," *Microwave Review*, vol. 19, pp. 3–14, 2013.

[3] A. Tiwari, "Fractal applications in electrical and electronics engineering," *International Journal of Engineering Science & Advanced Technology*, vol. 2, no. 3, pp. 406–411, 2012.

[4] B. Kattimani and R. R. Patil, "Bandwidth enhancement of microstrip antenna using fractal geometry for S-band applications," *SN Computer Science*, vol. 2, no. 4, pp. 282–288, 2021.

[5] K. Kavitha, R. P. Ganapathy, S. M. Ibrahim, and V. I. Aakash, "Design of microstrip fractal antenna for vehicle-to-vehicle communication," *Journal of Xidian University*, vol. 14, no. 8, pp. 1127–1137, 2020.

[6] V. V. Reddy, "Metamaterial Loaded Circularly Polarized Fractal Antenna for 2.4 GHz Frequency Applications," *IETE Journal of Research*, vol. 67, 2021.

[7] N. L. Nhlengethwa, P. Kumar, and K. Pradeep, "Fractal microstrip patch antennas for dual-band and triple-band wireless applications," *International Journal on Smart Sensing and Intelligent Systems*, vol. 14, no. 1, pp. 1–9, 2021.

[8] J. S. Abdaljabar, M. Madi, A. Al-Hindawi, and K. Y. Kabalan, "Design and fabrication of COVID-19 microstrip patch antenna for wireless applications," *Progress In Electromagnetics Research C*, vol. 118, pp. 125–134, 2022.

[9] E. A. M. Souza, P. S. Oliveira, A. G. D'Assunção, L. M. Mendonca, and C. Peixeiro, "Miniaturization of a microstrip patch antenna with a Koch fractal contour using a social spider algorithm to optimize shorting post position and inset feeding," *International Journal of Antennas and Propagation*, vol. 2019, pp. 1–10, Article ID 6284830, 2019.

[10] P. R. Rao, B. T. Madhav, CH. Deepthi et al., "Design and analysis of multi-band metamaterial antenna for wireless and ITO applications," *International Journal of Recent Technology and Engineering*, vol. 8, no. 1, pp. 334–340, 2019.

[11] U. Patel, M. Parekh, A. Desai, and T. Upadhyaya, "Wide Slot Tri-band Antenna for Wireless Local Area Network/Worldwide Interoperability for Microwave Access Applications," *John Wiley & Sons*, vol. 34, pp. 1–10, 2021.

[12] K. Gangwar and R. P. S. Gangwar, "Metamaterials: characteristics, process and applications," *Advances in Electronic and Electric Engineering*, vol. 4, no. 1, pp. 97–106, 2014.

[13] G. Singh, R. ni, and A. Marwaha, "A review of metamaterials and its applications," *International Journal of Engineering Trends and Technology*, vol. 19, no. 6, pp. 305–310, 2015.

[14] G. Geetharamani and T. Aathmanesan, "A Metamaterial Inspired Tapered Patch Antenna for WLAN/WiMAX Applications," *Wireless Personal Communications*, vol. 113, 2020.

[15] G. Geetharamani and T. Aathmanesan, "Design of Metamaterial Antenna for 2.4 GHz WiFi Applications," *Wireless Personal Communications*, vol. 113, 2020.

[16] A. Annou, S. Berhab, and F. Chebbara, "Metamaterial-fractal-defected ground structure concepts combining for highly miniaturized triple-band antenna design," *Journal of Microwaves Optoelectronics and Electromagnetic Applications*, vol. 19, no. 4, pp. 522–541, 2020.

[17] CH. Kumar and N. K. Muvvala, "A compact ultra-wide band rhombus shaped fractal antenna with metamaterial in the ground plane," *International Journal of Engineering and Advanced Technology*, vol. 8, no. 6, pp. 1349–1354, 2019.

[18] U. Patel and T. K. Upadhyaya, "Dual band planar antenna for GSM and WiMAX applications with inclusion of modified split ring resonator structure," *Progress in Electromagnetics Research Letters*, vol. 91, pp. 1–7, 2020.

[19] U. Patel and T. K. Upadhyaya, "Design and analysis of μ-negative material loaded wideband electrically compact antenna for WLAN/WiMAX applications," *Progress In Electromagnetics Research M*, vol. 79, pp. 11–22, 2019.

[20] U. Patel, T. K. Upadhyaya, A. Desai, R. Pandey, and K. Pandya, "Dual-band compact split-ring resonator-shaped fractal antenna with defected ground plane for sub-6-GHz 5G and global system for mobile communication applications," *International Journal of Communication Systems*, vol. 35, no. 7, pp. 1–12, 2022.

[21] A. Saedy, S. Saleh, and M. Yones, "Analyses and design of microstrip printed antennas using Galerkin theory," *Tishreen University Journal for Research and Scientific Studies - Engineering Sciences Series*, vol. 32, no. 4, pp. 195–210, 2010.

[22] Ch. Faten, B. Hafedh, E. Lassaad, and J. W. Tao, "Generalized scattering matrix method for analysis of cascaded uni-axial discontinuities," *ARPN Journal of Engineering and Applied Sciences*, vol. 11, no. 7, 2016.

[23] D. M. Pozar, *Microwave Engineering*, John Wiley & Sons, New York, 2008.

[24] C. A. Balanis, *Antenna Theory: Analysis and Design*, John Wiley & Sons, New York, 2005.

[25] A. Saedy, S. Saleh, and S. Ali, "Design and analysis of a wideband printed fractional antenna for medical and internet equipments applications," *Tishreen University Journal for Research and Scientific Studies - Engineering Sciences Series*, vol. 43, no. 2, pp. 235–250, 2021.

[26] F. G. Hu, J. Song, and T. Kamgaing, "Modeling of multilayered media using effective medium theory," in *Proceedings of the IEEE Electrical Performance of Electronic Packaging and Systems*, pp. 225–228, Austin, TX, USA, October 2010.

[27] T. Zhao, *Effective Medium Modeling and Experimental Characterization of Multilayer Dielectric with Periodic Inclusion*, Iowa State University, Ames, Iowa, 2015.

[28] K. V. Arshad, A. K. Bilal, A. R. Mohamad, M. N. Iqbal, and H. T. Chattha, "Metamaterial-Inspired Electrically Compact Triangular Antennas Loaded with CSRR and $3 * 3$ Cross-Slots for 5G Indoor Distributed Antenna Systems," *Micromachines*, vol. 13, pp. 1–16, 2022.

[29] K. P. Nitish and J. Kavitha, "Design and Simulation of Microstrip Fractal Patch Antenna," *Materials Science and Engineering*, vol. 1070, pp. 1–16, 2021.